Synthesis of catalytic materials in flames: opportunities and challenges

Rajesh Koirala,[a] Sotiris E. Pratsinis[a] and Alfons Baiker*[b]

The proven capacity of flame aerosol technology for rapid and scalable synthesis of functional nanoparticles makes it ideal for the manufacture of an array of heterogeneous catalysts. Capitalizing on the high temperature environment, rapid cooling and intimate component mixing at either atomic or nano scale, novel catalysts with unique physicochemical properties have been made using flame processes. This tutorial review covers the main features of flame synthesis and illustrates how the physical and chemical properties of as-synthesized solid catalytic materials can be controlled by proper choice of the process parameters. Gas phase particle formation mechanisms and the effect of synthesis conditions (reactor configuration, precursor and dispersion gas flow rates, temperature and concentration fields) on the structural, chemical and catalytic properties of as-prepared materials are discussed. Finally, opportunities and challenges offered by flame synthesis of catalytic materials are addressed.

Key learning points

I. Main features of flame synthesis methods.

II. Particle formation mechanisms.

III. Tuning material properties by manipulating their flame synthesis conditions.

IV. Influence of materials properties such as chemical composition, crystallinity particle size, specific surface area and acidity/basicity on catalysts' performance.

V. Opportunities and challenges in flame synthesis of catalysts.

1. Introduction

Flame aerosol technology for synthesis of nanoparticles, *e.g.* carbon black, dates back to the beginning of human civilization as can be seen in the remnants of numerous art works. The Ancient Chinese were among the first to produce them in larger quantity.[1] Industrial scale production of carbon black started with the discovery of its use in reinforcing rubber, thus drastically increasing its demand especially by the motor vehicle industry.[1] So carbon black is the largest by volume and value flame-made commodity. Nowadays, using this technology a few other commodities are produced such as optical waveguides, pigmentary TiO_2, fumed SiO_2, Al_2O_3 and other oxides[1] and even specialty chemicals (*e.g.* nanofluids). Due to its versatility and ease of materials production, flame synthesis is displacing older technologies,[2] *e.g.* the "chloride" *versus* the "sulfate" process
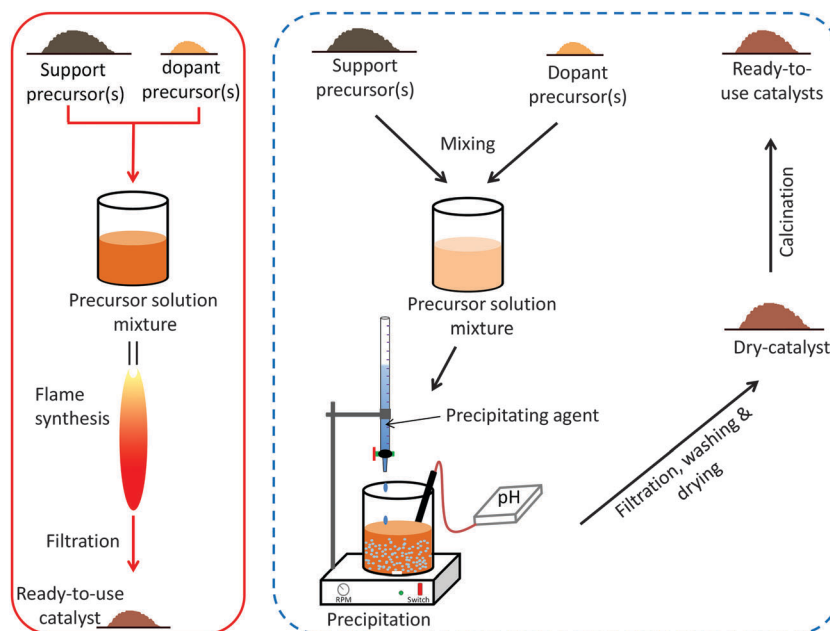
for pigmentary TiO_2. Industries like Evonik, Cabot, Dupont *etc.* produce in large scale ceramic powders in flames indicating the scale-up potential of this technology for a wide range of materials production.[2]

To start with, the widely-used photocatalytic material, nano-TiO_2 P25 by Evonik, is made by oxy-hydrogen flames.[2] In addition to metal oxides, bi- or multi-metal oxides as well as oxide-supported noble metals that are of prime interest in catalysis, such as ZrO_2, Fe_2O_3, ZnO, SnO_2, TiO_2/SiO_2, SiO_2/Al_2O_3, Pt/TiO_2, $LaBO_3$ (B = Co, Mn, Fe) and $Pd/La_2O_3/Al_2O_3$ have been made already using flame aerosol technology.[3] Flame methods offer a couple of attractive features that are not achievable with classical wet-chemistry methods. A detailed overview of classical catalyst preparation methods such as co-precipitation, impregnation, sol–gel and hydrothermal syntheses is provided in an all-embracing review.[4] As a representative example, Fig. 1 compares the main steps involved in a classical wet-chemistry preparation (co-precipitation) and flame synthesis of a catalyst. A striking difference between the classical preparation and flame aerosol synthesis is the number of steps involved. Wet-chemistry methods generally consist of various time consuming steps, while the flame methods

[a] *Particle Technology Laboratory, Department of Mechanical and Process Engineering, ETH Zurich, Sonneggstrasse 3, CH-8092 Zurich, Switzerland*

[b] *Department of Chemistry and Applied Biosciences, ETH Zurich, Hönggerberg, HCI, Vladimir-Prelog Weg 1, CH-8093 Zurich, Switzerland. E-mail: baiker@chem.ethz.ch; Fax: +41 44 632 11 63; Tel: +41 44 632 31 53*

This journal is © The Royal Society of Chemistry 2016

Chem. Soc. Rev., 2016, **45**, 3053–3068 | 3053

Fig. 1 Comparison of flame synthesis with classical wet-preparation method (co-precipitation) of catalysts. Ready-to-use catalysts can be produced in a single step using flame aerosol technology (red bracket), whereas wet-methods (broken blue bracket) often require multiple steps, sometimes taking days, to produce them. Depending on the application (reactor type) a possible forming step (*e.g.* extrusion, granulation, pelletizing) at the end of both preparation routes may be necessary, which has not been indicated in the schemes. Adapted from ref. 3 with permission from Elsevier.

facilitate rapid single step synthesis. *In situ* calcination during the high temperature production alleviates the need of post thermal treatment. Moreover, flame-made catalysts require no solvent-intensive washing that increases the chance of altering the catalyst composition due to leaching of components. Additionally, flame synthesis affords continuous production, while wet-chemistry routes are usually batch processes. Rapid quenching of the flame-made particles gives access to the formation of metastable phases and thus catalytic materials with distinctly different properties compared to wet-chemistry

made materials can be produced. Flame aerosol technology is highly versatile as it can easily tune catalyst characteristics such as specific surface area (SSA), particle size and crystallinity through its process parameters.[5] Moreover, spatial and also preferential deposition of the active materials can be achieved by multiple flames in a single step.[6] Some restraints for the production of catalysts by flame methods arise from the fact that suitable precursors are relative expensive and highly crystalline and porous materials are difficult to produce. Moreover, not all precursors are easily mixed, explosive precursors mixtures and

Rajesh Koirala (1984, Nepal) obtained his BSc in chemical engineering from Texas A&M University, USA (2009) and his MSc in the same field from the University of Cincinnati, USA (2012). He is currently doing his PhD under the supervision of Prof. Sotiris E. Pratsinis at Particle Technology Laboratory, ETH Zurich. He received the AIChE Environmental Division Graduate Student Best Paper award (2012) for his contribution

Rajesh Koirala

towards the development of novel flame-made CO_2 sorbents. His current research focuses on the development of novel catalysts utilizing flame spray pyrolysis method, for upgrading alkanes to high-value products.

Sotiris E. Pratsinis has a diploma in chemical engineering from the Aristotle University of Thessaloniki, Greece (1977) and a PhD from University of California, Los Angeles (1985). He was professor of chemical engineering at the University of Cincinnati (1985–2000) until he was elected professor of Process Engineering & Materials Science at ETH Zurich (1998). There he teaches Mass Transfer, Micro- & Nanoparticle Technology, Nano-

Sotiris E. Pratsinis

scale Engineering and Combustion Synthesis of Materials. His research program on particle dynamics focuses on the fundamentals of aerosols and reactor design for synthesis of materials for catalysis, gas sensors and life science applications.

3054 | *Chem. Soc. Rev.*, 2016, **45**, 3053–3068

This journal is © The Royal Society of Chemistry 2016

conditions should be considered and in some cases products of incomplete combustion could be present.

Applications of flame-made nanomaterials can be found in catalysis, sensors, biomaterials, ceramics, composites and bioimaging.[7] In catalysis, Strobel et al. reviewed[3] the use of flame-made catalysts for photocatalysis, epoxidation, selective catalytic reduction of NO_x and CH_4 combustion. A follow-up review by Schimmoeller et al.[8] showed the fast growing production and utilization of flame-made catalysts focusing on V_2O_5-based catalysts and their structural and chemical properties in comparison to those prepared by classical wet methods. The growing interest in flame aerosol synthesis of catalysts can be ascribed primarily to its flexibility, speed and scalability.

The purpose of this tutorial review is to provide a holistic view on flame methods and their potential for controlling physical and chemical characteristics (e.g. surface area, particle size, crystal structure, chemical and phase composition etc.) of catalytic materials. We will start with a brief description of particle formation mechanisms in different flame reactors. Later on, the influence of synthesis conditions on the physico-chemical properties of as-prepared materials and their effect on the catalyst performance is illustrated using various examples. At last, future opportunities offered by flame techniques for the preparation of sophisticated materials for catalysis will be discussed.

2. Experimental conditions of flame synthesis and their influence on material properties

2.1 Particle formation mechanism

During flame aerosol synthesis, particle formation follows two main routes: droplet-to-particle and gas-to-particle[2] conversion

resulting in particles by top-down or bottom-up processes, respectively. Depending on the state of the metal precursor, we distinguish vapor-fed and liquid-fed flame synthesis processes (Fig. 2a).[3] Vapor-fed flame processes lead to particles solely by gas-to-particle conversion while liquid-fed ones may involve particle formation by both routes.

In vapor-fed aerosol flame synthesis (VAFS), gaseous precursors (e.g. $TiCl_4$, SiH_4 vapors) are fed to the flame resulting in product particles by nucleation, surface growth and/or condensation that grow further by coagulation–agglomeration. Such particles are aggregates (chemically-bonded primary particles) and agglomerates (physically-bonded primary particles). Their state depends on material properties and residence time in the
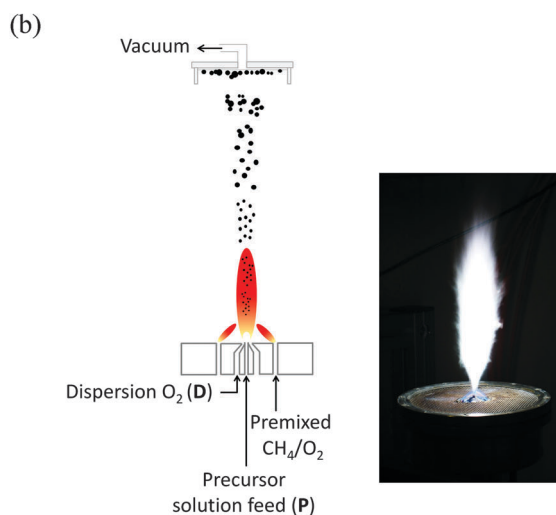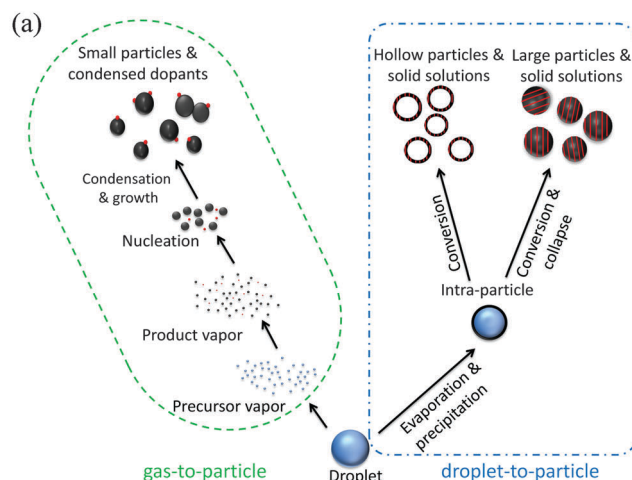
Fig. 2 Schematic of (a) possible particle formation pathways during the aerosol synthesis and (b) FSP setup for nanoparticles synthesis and a picture of the flame during nanoparticle production. Large or hollow particles are formed during FASP synthesis, whereas only partly in FSP. Mainly, smaller particles are formed from FSP and VAFS where precursor droplets are transformed to vapor which after combustion, nucleation, surface growth and condensation produce nanoparticles. Metal oxide nucleation and solid solution formation is governed by their melting temperatures. Adapted from ref. 3 with permission from Elsevier.

Alfons Baiker studied chemical engineering at ETH Zurich and earned his PhD degree in 1974. After several postdoctoral stays at various universities he finished his habilitation at Stanford University (California) and returned to ETH in 1980, where he started his own research group focusing on heterogeneous catalysis and reaction engineering. He moved up to the ranks to become Full Professor in 1990. His research interests, documented in more than 900 publications in refereed journals and numerous patents, are centered on catalyst design and novel catalytic materials, mechanisms and kinetics of catalytic surface processes, chiral surfaces, asymmetric hydrogenation, selective oxidation, environmental catalysis, operando spectroscopy, and the application of super-critical fluids and ionic liquids in catalysis.

Alfons Baiker

flame.[9] This is an industrially applied process for the synthesis of photocatalytic TiO_2 and catalyst supports (SiO_2, Al_2O_3 etc.) as well as pigmentary TiO_2 and fumed silica, alumina etc. In multicomponent catalysts, metal oxides (refractories) with high melting point condense out first while other components/species (noble metals or soft oxides) precipitate or form on them according to their melting temperature (e.g. V_2O_5 on TiO_2 for NO_x reduction)[10] or surface reactions. Supported catalysts such as $Cu/ZnO/Al_2O_3$ for methanol synthesis, Pt/TiO_2 for SO_2 oxidation and TiO_2/SiO_2 for epoxidation of cyclohexenol have been already produced via this technique.[3]

In liquid-fed flames we distinguish if the supporting fuel is mixed with the metal precursor (flame spray pyrolysis, FSP)[11] or it is provided separately (flame-assisted spray pyrolysis, FASP).[12] In both, the metal precursors are sprayed into fine droplets that should evaporate to precursor vapor for nanoparticle synthesis by gas-to-particle conversion. In FSP,[13] the precursor droplets contain the fuel that evaporates and burns to drive particle formation. This phenomenon greatly facilitates the one-step synthesis of noble metal clusters on catalytic supports, e.g. Pt/Al_2O_3 for enantioselective hydrogenation reaction.[14] Due to its compact and easy operation, the FSP technique for synthesis of catalysts[3] has been popular and gaining recently lots of interest from industry.[15] In FASP, the fuel combustion is decoupled from the precursor droplets. Typically H_2 or hydrocarbon gases are burned and the precursor droplets are sprayed into their flame. In both FSP and FASP, droplets could be converted to either hollow or large micron- or nano-particles and/or solid solutions of varying morphologies and sizes. Hollow particles are formed due to precipitation of precursor around the droplet before the evaporation of the solvent. Larger particles are the result of drying, collapse and densification of droplets due to insufficient enthalpy for the conversion of liquid solvent to vapor before precursor surface precipitation. Ideally, precursor vapor is generated during FASP and FSP, which after chemical reaction, give particles of nanometer size as in VAFS. Quite a few catalysts have been produced by FASP (e.g. $SrMnO_3$, $SrTiO_3$ and MoO_3/TiO_2) and FSP (e.g. $LaMnO_3$, $LaCoO_3$, Au/TiO_2 and Ag/ZnO) and have been evaluated already for catalytic reactions such as photocatalysis, CH_4 combustion and CO oxidation.[3]

2.2 Reactor configurations

VAFS reactors require vapor precursor that is combusted or oxidized on its own or assisted by a hydrocarbon or H_2/O_2 flame to produce nanoparticles. High cost and difficulty in finding volatile precursors make VAFS challenging for catalyst synthesis that requires several components. Moreover, in synthesis of multicomponent particles by VAFS, it is difficult to achieve homogeneous distribution of metal oxides due to differences in their precursor volatility.

The FSP and FASP reactor configurations overcome the necessity of volatile metal precursors as they utilize precursors that dissolve typically in combustible (FSP) and noncombustible (FASP) solvents. As a result, virtually all elements in the periodic table can be used by liquid-fed flame synthesis processes. Both configurations are similar, differences exist mainly in their

operating principle. The FASP utilizes low enthalpy content or non-combustible aqueous solutions of typically nitrate and acetate precursors that are rather cheap. Therefore they require an external source of energy in the form of hydrocarbon or H_2/O_2 flames to drive droplet/gas-to-particle conversion. The FASP[12] produces nanometer to submicron sized particles, depending on the applied combustion energy.

On the other hand, FSP, which was first introduced by Sokolowski et al.[11] for synthesis of Al_2O_3 is quite similar in concept to carbon black synthesis by the furnace process[7] and leads readily to nano-sized particles by gas-to-particle conversion. During FSP,[13] the precursor solution is fed at the center of the reactor (Fig. 2b), e.g. with a syringe pump, dispersed by high velocity gas (e.g. O_2) creating a fine spray of droplets that is ignited and stabilized by a pre-mixed flame. After combustion, particles are formed as in VAFS. Worth noting is that, more than 50% of energy is contributed by the liquid precursor solution during the combustion process in FSP.[3] Each reactor configuration has its own merit but FSP is generally preferred due to its capacity to produce nano-sized homogeneous particles and its compact operation provided that appropriate precursor–solvent mixtures are identified for a given catalyst composition.

## 2.3 Flame parameters for catalyst synthesis

Precursor concentration, fuel, mixing, oxidant, entrainment, precursor/dispersion flow rate ratio (P/D) and precursor solution composition are some of the process parameters that affect product properties and in particular primary particle and crystallite sizes that frequently affect catalytic performance. In VAFS, precursor concentration in the carrier gas (e.g. O_2, Ar) is primarily controlled by evaporator, whereas carrier gas flow rate can also be used in regulating the rate at which precursor vapor is fed to the flame. Moreover, fuel (H_2 or hydrocarbon) and oxidant flow rates and their mixing influence the product particle properties.[2]

Fig. 3a shows the effect of titanium isopropoxide (TTIP) flow rates (1.6–26 g h^{-1}) on the average particle diameters (d_p, $d_{Anatase}$ and d_{Rutile}) and anatase content of TiO_2 at constant CH_4, carrier-gas (Ar) and O_2 flow rates.[16] The particle and crystallite sizes increased with increasing TTIP flow rate until about 16 g h^{-1} and remained nearly constant at higher rates. Increasing TTIP flow rate increases both concentration and flame temperature that accelerate particle growth by coagulation and sintering.[2] However, growth in primary particle size (d_p) slows down at higher TTIP flow rates, here (>16 g h^{-1}) as particle growth by sintering is inversely proportional to particle size requiring much longer residence times at high temperature with increasing particle size.[9] Anatase TiO_2 content decreased significantly (85–18 wt%) with increasing TTIP flow rates (1.6–26 g h^{-1}) due to increasing O_2 deficiency that favors rutile formation,[16] highlighting its importance in the flame aerosol synthesis.

Fig. 3b shows the influence of hydrocarbon (e.g. CH_4) flow rate and VAFS burner configurations on the primary particle diameter of TiO_2 at a $TiCl_4$ flow rate of 1.6×10^{-4} mol min^{-1}.[5] The d_p increased with increasing CH_4 flow rate for both gas mixing patterns (Flame A and B). However, much bigger and
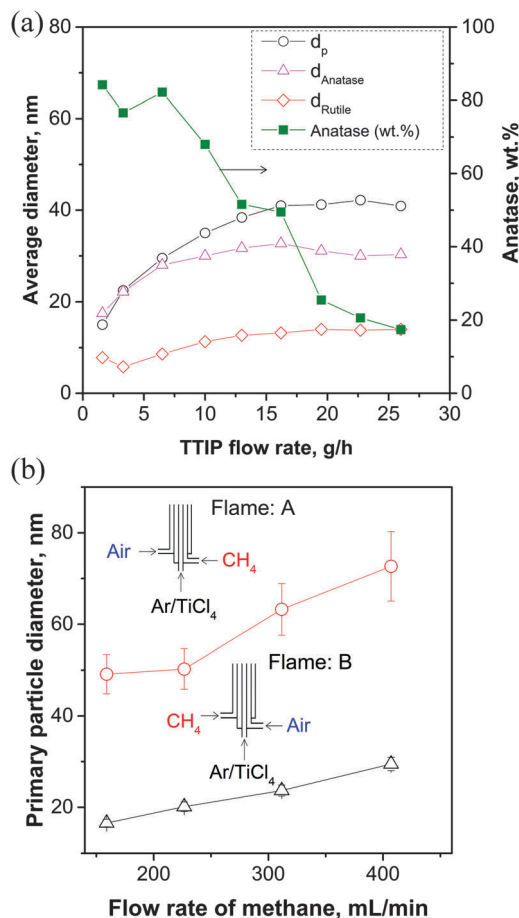
Fig. 3 (a) Primary particle diameter (circles, left axis), anatase (triangles, left axis), and rutile (diamonds, left axis), phase composition (squares, right axis) of TiO$_2$ powders made in flames with 2 L min^{-1} O$_2$ flow rate and the quenching nozzle placed at 5 cm above the diffusion burner (VAFS) for TTIP flow rates of 1.6 to 26 g h^{-1} [16] and (b) Primary particle diameter of TiO$_2$ particles made in diffusion burner (VAFS) with two configurations: flame A (red symbols) and B (black symbols) as a function of CH$_4$ flow rate at constant 3.8 L min^{-1} air flow rate.[5] Adapted from ref. 16 and 5 with permission from John Wiley & Sons and Elsevier.

less aggregated particles were formed in classic diffusion flames (A) than in inverse (or double) diffusion flames (B). In flame A high concentration of newly formed particles experience high temperature from CH$_4$ combustion that promotes coalescence (or sintering) before they get cooled or diluted by air, whereas in flame B the sequence is reversed. Sintering of the particles can be further suppressed by increasing the air flow rate, which dilutes and cools the flame.[5] Controlling the oxidant (air or O$_2$) flow rate, which in turn affects the particle residence time, TiO$_2$ catalysts containing 10 wt% V$_2$O$_5$ with a wide range of SSA were prepared.[10] Their specific surface area could be increased from 23 to 120 m^2 g^{-1} by increasing the O$_2$ flow rate from 2 to 10 L min^{-1} in a diffusion flame and a homogeneous distribution or coating of vanadia on TiO$_2$ could be achieved.[10] This change in SSA significantly influenced the selective catalytic reduction of NO that will be further discussed in Section 3.3.

High temperature residence time, a dominant characteristic of flame synthesis that determines the extent of particle growth

(by coalescence and sintering), can be controlled also by applying an electric field in the flame.[2] The average primary particle diameter of TiO$_2$ decreased with increasing the field strength using needle or plate (corona discharge) electrodes. The field generated by the electrodes across the flame reduces the particle residence time in the high temperature region. Moreover, it also charges the newly formed particles, which creates electrostatic repulsion and dispersion. Both phenomena favor resistance towards particle growth resulting in smaller primary particles.

Concepts similar to VAFS are utilized in both FSP and FASP where particle properties are controlled easily by P and D, which are equivalent to changing simultaneously both precursor/fuel concentrations and oxidant ratio in VAFS. The degree of dispersion, high temperature particle residence time and extent of combustion are closely related to the P/D ratio. Its effect is quite similar for most materials during their FSP synthesis, especially when particle formation takes place solely by gas-to-particle conversion as in VAFS.[13] High surface area materials can be made by decreasing the P/D ratio which results in shorter visible flames thus lowering the particle residence time in the high temperature zone and slowing down particle growth (Fig. 4). The opposite effect occurs at higher P/D ratios. This has been well demonstrated in the synthesis of various catalytic materials.[3,8] However, this trend does not always hold[13] especially when there are products of incomplete combustion.[17] This can be mitigated sometimes by utilizing sufficient combustion energy e.g. by using high enthalpy solvents.[13]

Additionally, flame-made particle characteristics can be tuned at constant P/D ratio by enclosing the FSP with a tube, which blocks air entrainment to the flame spray jet, thus preventing the cooling of the flame (Fig. 4, inset).[18] Moreover, particle size can also be controlled by varying the length of such tube and essentially controlling such high temperature residence time.
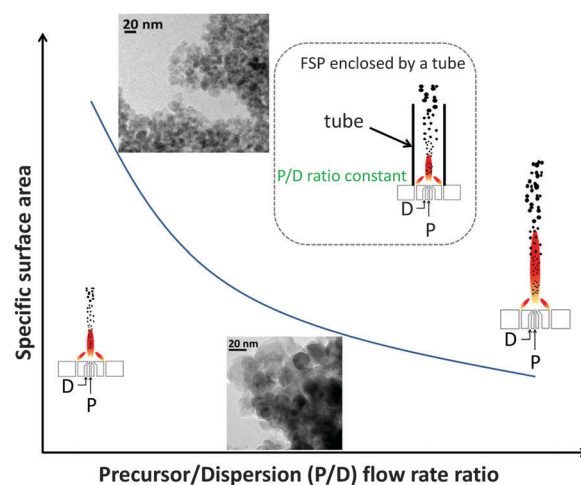
Fig. 4 Conceptual schematic of effect of precursor/dispersion (P/D) ratio on specific surface area (SSA) of material. SSA decreases with increasing the P/D ratio. Furthermore, particle size can also be controlled by addition and changing the length of the tube and/or air entrainment by lifting the tube (see scheme in the middle) at constant P/D ratio. Adapted from ref. 38 with permission from Elsevier.
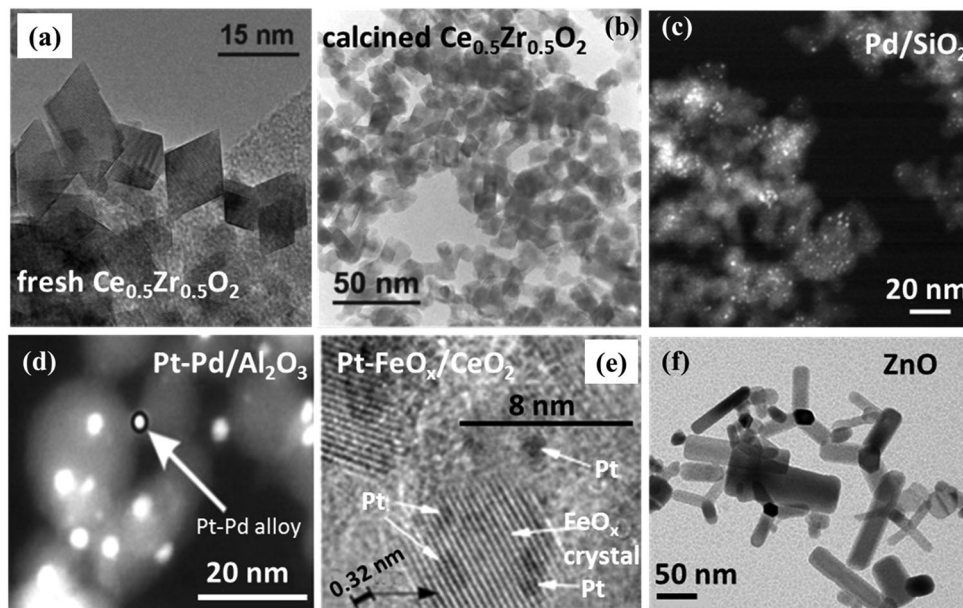
Fig. 5 Electron micrographs of the structure of various flame-made catalytic materials. Nanocrystals of (a) fresh and (b) calcined (900 °C for 2 h in air) $Ce_{0.5}Zr_{0.5}O_2$. Lattice fringes indicate well developed single crystals in most cases and calcination affords crystalline particles of similar size.[19] (c) Pd supported SiO_2 where Pd was well dispersed with a size ranging from 1–2 nm.[24] (d) Al_2O_3 supported Pt–Pd catalyst where Pt–Pd coexisted as an alloy as confirmed by EDXS and EXAFS analysis.[46] (e) Pt–FeO_x/CeO_2 catalyst with Pt residing in FeO_x crystal hinting to strong interaction between them.[49] (f) Flame-made ZnO nanorods with length and diameter as high as 100 nm and 50 nm, respectively.[53] Adapted from ref. 19, 24, 46, 49 and 53 with permission from Royal Society of Chemistry, Elsevier and Springer.

The FSP or FASP solvent composition can critically affect the product catalyst characteristics. In FSP synthesis of CeO_2–ZrO_2, precursor solutions derived from the mixture of lauric-acetic acid gave highly crystalline $Ce_{0.5}Zr_{0.5}O_2$ (Fig. 5a). In contrast, a product containing ceria rich and zirconia-like phases was obtained when mixing iso-octane, acetic acid and 2-butanol.[19] In the latter precursor solution spray, rapid release of all liquid solvent from droplets takes place (due to low boiling point, around 100 °C) leaving lumps of precursor salts. Due to difference in the decomposition rate of the two salts inhomogeneous distribution of these materials occurs resulting in products of different compositions. The highly crystalline $Ce_{0.5}Zr_{0.5}O_2$ still remained open with only few contacts between particles, thus improving sintering-resistance as demonstrated by the good thermal stability of $Ce_{0.5}Zr_{0.5}O_2$ even when calcined at 900 °C for 2 h in air (Fig. 5b)[19] indicating its potential application in high temperature catalytic reactions, *e.g.* the partial oxidation of CH_4.

2.4 Temperature

Temperature strongly affects the characteristics of flame-made catalysts. Flame aerosol synthesis, involves combustion of precursors to produce materials, and as a consequence strong temperature profiles are established in the reactor, *e.g.* in the SiO_2 synthesis flame.[13] These profiles highly depend on the applied process parameters such as precursor composition, solvent and oxidant gas (O_2/air) and have a significant effect on the final structural and chemical properties of the materials.

Generally, the average flame temperature is around 2000 °C just above the nozzle.[13] Usually it increases slightly above the

burner as the precursor/solvent are consumed and then decreases with further distance away from the burner as it mixes with entrained oxidant or sheath gas. These temperature profiles can vary with solvent type (*e.g.* ethanol or xylene). The highest measured temperature for pure ethanol and xylene flames were ∼2700 °C and ∼3400 °C, respectively.[20] This temperature difference can be related to the lower flame temperature resulting from stoichiometric combustion of O_2 with the former solvent compared to that from the latter. Temperature profiles obtained from a simulation model showed excellent agreement with experimental values especially for larger heights, which opens up the possibility of determining flame temperature computationally for a wide range of materials synthesis.[20]

3. Particle properties relevant for catalysis

3.1 Chemical composition

The chemical composition is a key parameter in the design of catalysts. Flame methods are versatile as regards tailoring of elemental composition. Limitations exist only concerning solubility of precursors in a single miscible solvent solution and potential toxicity of vapors, *e.g.* nickel tetracarbonyl formation in the flame when employing nickel precursors. In such cases special safety measures have to be taken, *e.g.* particle production inside the glove box.[21] Purity of the catalyst composition is essential as even trace amounts (in ppm range) of impurities influence catalytic performance. Wet-synthesis processes generally require multiple steps thereby increasing

the chance of losing active elements and also possible contamination from residues or production equipment. In contrast, flame aerosol synthesis can produce materials with well specified composition and high purity.[2,7]

Transition metal impurities (Co, Cr, Mn and Fe) were added deliberately in the ppm range in the flame synthesis of TiO_2/SiO_2 epoxidation catalysts lowering their selectivity to the epoxide compared to that of pure catalysts (Fig. 6a).[22] The drastic reduction of olefin selectivity with increasing Cr addition (>3 ppm) was due to leaching of Cr into the reaction solution, leading to homogeneous catalysis, catalyzing the substrate conversion to the corresponding ketone. This example shows that doping in the ppm range is easily achievable with flame synthesis and highlights the importance of catalyst purity.

The acidity/basicity of catalysts can be tuned by their chemical composition. Generally, this is achieved by adding components that possess acidic or basic sites, or by combining

oxides which upon interaction form active sites with enhanced acidity, e.g. by combining SiO_2 and Al_2O_3. This has been exemplarily shown for Pt catalysts supported on mixed SiO_2–Al_2O_3 having acidic sites and for Pt/Cs_2O possessing basic sites.[23] Fig. 6b shows that by increasing the SiO_2 content in Pt/Al_2O_3, the ratio of Brönsted/Lewis acid sites (B/L) can be decreased. Increasing the B/L ratio directly affected both the methyl benzoylformate and ketopantolactone hydrogenation reaction rates and all SiO_2–Al_2O_3 supported Pt catalysts showed higher activity than those on pure Al_2O_3 (Fig. 6c). Moreover, an optimal B/L acid ratio (around 0.25) was achieved by adding 30 wt% SiO_2 that exhibited the highest enantioselectivity for both reactions.[23] The change in acidity of the support also influences the electronic properties of the loaded noble metals such as Pt[23] and Pd.[24] These changes in the properties of noble metals can be a decisive factor determining their catalytic behavior. Similarly, silica addition to ZrO_2 introduced Brönsted acid sites that enhanced the mandelate yield from about 8%
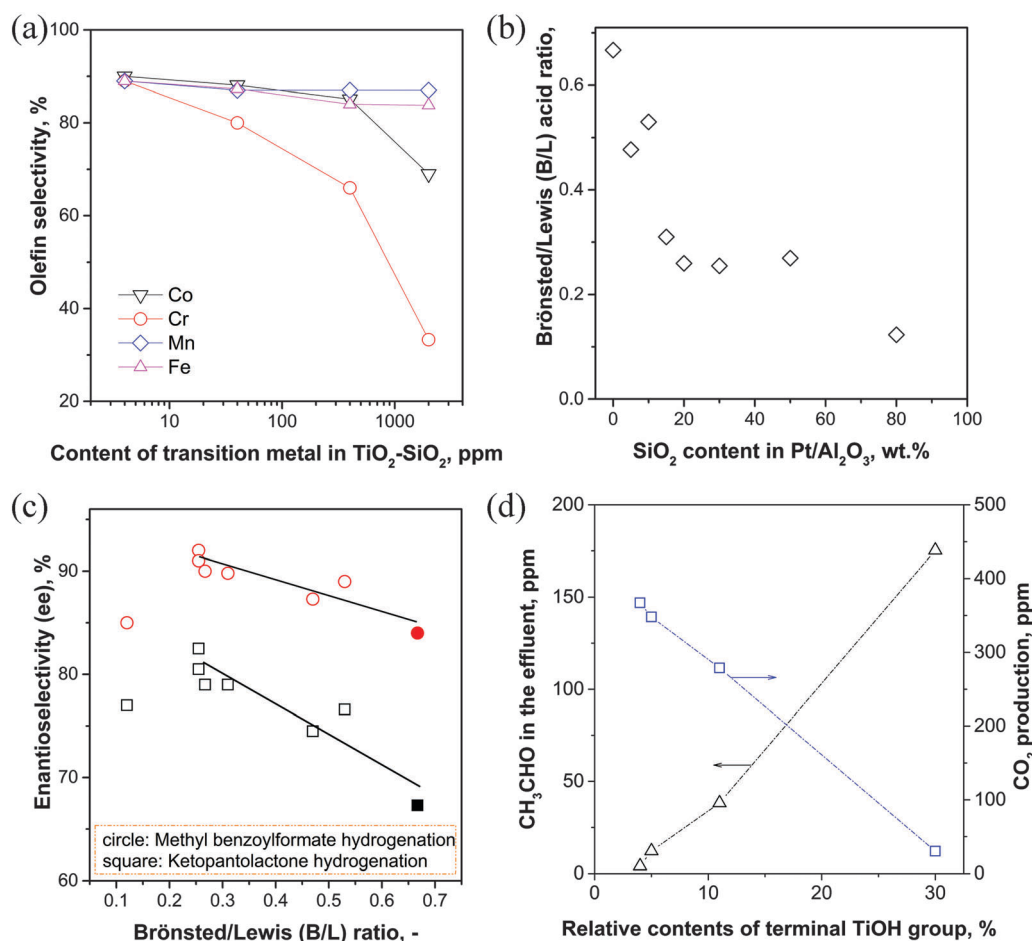
Fig. 6 (a) The selectivity of epoxide formation related to alkene consumption for transition metal-doped TiO_2–SiO_2. Doping with Cr and Co reduce the efficiency of the alkene usage, while incorporation of Mn and Fe does not lead to significant loss of alkene reactant at dopant levels of up to 2000 ppm. Cr exhibits the most pronounced effect, as it leaches into the reaction mixture, converting most of the substrate to the corresponding ketone instead of epoxide formation.[22] (b) Effect of SiO_2 on Brönsted/Lewis (B/L) ratio of Pt/Al_2O_3 catalysts and (c) its influence on enantioselectivity, Pt/Al (filled symbols) and Pt/Al–Si (open symbols).[23] (d) Variation of acetaldehyde concentration in effluent after UV photodegradation and CO_2 produced under steady-state conditions with the relative content of terminal TiOH groups estimated by ^{1}H MAS NMR studies (initial acetaldehyde concentration = 183 ± 10 ppm).[26] Adapted from ref. 22, 23 and 26 with permission from Royal Society of Chemistry and Elsevier.

(for pure ZrO_2) up to 52–67% in the mixed oxides in the hydrogenation of phenylglyoxal to ethyl mandelate.[25]

Control over hydroxyl (OH) groups on FSP-made TiO_2[26] and Pt/TiO_2[27] by doping Cu and fluorine (F) has been recently reported. The performance over F-doped TiO_2 was superior to that of Cu-doped TiO_2 in the photodegradation of acetaldehyde, as evidenced by the CO_2 production (Fig. 6d).[26] This difference in the activity could be directly related to their relative content of terminal TiOH, where former had the lowest ($\sim$4%) and latter had the highest ($\sim$30%) values. During the photocatalytic hydrogen production, an improvement of the performance was observed (from 19.1 to 22 mmol h^{-1} g_{cat}^{-1}) over Pt/TiO_2 after addition of 5 wt% F, which was attributed to an increase in the population of surface OH groups.[27] At higher loadings, the H_2 production rate decreased due to the introduction of structural defects hindering the interface electron transfer.

3.2 Multi-metal systems

Multicomponent materials such as mixed oxides have been widely investigated in various catalytic reactions because they offer fascinating possibilities for tailoring catalyst properties. FSP has been successively used for producing various high surface area, nonporous, mixed metal oxide nanopowders of different composition consisting of CeO_2–Al_2O_3, CeO_2–ZrO_2, CeO_2–ZrO_2–Al_2O_3, CoO–Al_2O_3, NiO–Al_2O_3 and ZrO_2–Al_2O_3.[28] High-throughput screening as well as continuous flow catalytic studies were applied to assess the catalytic performance of these mixed oxides for NO_x reduction and propane/propene oxidation. A set of $Ce_{1-x}Zr_xO_2$ and Al–$Ce_{1-x}Zr_xO_2$ nanopowders were shown to exhibit good catalytic activity for both NO_x reduction and propane/propene oxidation. Interestingly, all of these Pt-free catalysts showed activities comparable to traditional Pt/Al_2O_3 catalysts. In a later study, the same group describes the synthesis of $Ce_xZr_{1-x}O_2$ and $(Ce_{0.7}Zr_{0.3}O_2)_x(Al_2O_3)_{1-x}$ core–shell nanopowders.[29] These studies, among others, demonstrate that complex metal mixed oxides can be produced with good control of stoichiometry and phase purity using FSP. Beside their use as active component, the application of such mixed metal oxides as supports is also attractive due to their high thermal stability, *e.g.* $Ce_{0.5}Zr_{0.5}O_2$ (Fig. 5a and b).[19]

Flames are suitable for the rapid and single step synthesis of perovskites. These catalysts have shown high performance in CH_4 combustion (over $LaCoO_3$),[30] one among several other catalytic reactions, where high thermal stability and oxygen carrying capacity are important. Addition of an element into the perovskite structure can create partial metal ion substitution, thereby improving the catalytic activity, as *e.g.* in Ag-doping of $LaMnO_3$ (Fig. 7a).[31] Flameless combustion of CH_4 was improved distinctly with increasing Ag substitution of La in $LaMnO_3$ made by both flame and sol–gel method, with the former showing higher catalytic activity. The high activity of the flame-made catalysts was attributed to their high SSA, which facilitates the rapid oxygen transfer from bulk to surface and *vice versa*, resulting in high oxygen availability and faster regenerability. Moreover, temperature programmed reduction (TPR) showed that partial substitution of La by Ag decreased the
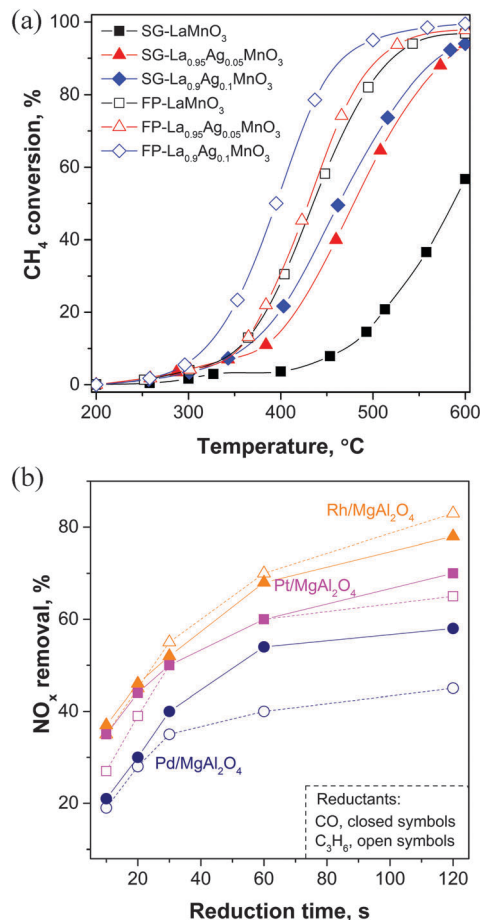

Fig. 7 (a) Catalytic activity of fresh perovskite catalysts produced using flame pyrolysis and sol–gel.[31] (b) NO_x storage–reduction (NSR) during lean-rich cycling at 350 °C over 1 wt% $M/MgAl_2O_4$ (M = Pt, Pd, or Rh) with different duration of rich period using CO and C_3H_6 as reductant. The NSR cycles were carried out with 360 s lean and 10, 20, 30, 60 and 120 s rich periods and plotted after 10 steady cycles.[32] Adapted from ref. 31 and 32 with permission from Royal Society of Chemistry and Elsevier.

onset of the first reduction peak and enlarged the Mn reduction range also contributing to the higher catalytic activity.

Spinels (*e.g.* $MgAl_2O_4$) have been widely applied as catalyst supports, apart from their usage in other fields such as sensors, due to their high thermal stability. Generally, active materials such as noble metals (Pt, Pd, Rh)[32] and/or transition metals (Mn, Fe, Co)[33] are loaded on spinels depending on catalytic application. Noble metal loading did not influence the spinel structure of $MgAl_2O_4$ and high dispersion was achieved for Rh compared to Pt and Pd. Therefore, the high NO_x removal activity of $Rh/MgAl_2O_4$ storage–reduction catalysts can be attributed to the high Rh dispersion and the activity could be further improved by changing the reductant from CO to C_2H_6, during regeneration (Fig. 7b). The wet synthesis of these noble metal-loaded $MgAl_2O_4$ catalysts generally requires two separate steps: synthesis of $MgAl_2O_4$ and later impregnation of noble metal(s), both requiring post thermal pretreatments, costing time and leading to lower SSA of the catalyst.

3060 | *Chem. Soc. Rev.*, 2016, **45**, 3053–3068

This journal is © The Royal Society of Chemistry 2016

These examples show the unique opportunity of flame aerosol technology to produce materials with high SSA in a rapid single step, while maintaining other important properties. Additionally, high SSA (174 to 212 m^2 g^{-1}) ternary spinels (e.g. MgAl$_{2-x}$M$_x$O$_4$, where M = Mn, Fe, Co) can also be formed by flame aerosol methods exhibiting high resistance towards sintering during catalytic CH$_4$ combustion.[33] Flame aerosol synthesis of these types of ternary spinel catalysts is possible due to the intimate mixing in the flame of the constituents (elements) on atomic scale. In contrast, if required, the Mn, Fe and Co loaded MgAl$_2$O$_4$ catalysts can be synthesized utilizing two nozzles, where the dopant resides on the well-structured spinel structure, as will be discussed in Section 3.6. Flame synthesis of different combination of WO$_3$/CeO$_x$–TiO$_2$ improved the surface Ce^{3+} concentration, which together with homogeneous coverage of particles (e.g. Ce–Ti) by amorphous WO$_3$ resulted in high NH$_3$-SCR activity comparable to that of the widely used wet-made V$_2$O$_5$–WO$_3$/TiO$_2$ catalysts. However, after hydrothermal aging the flame-made catalysts exhibited much higher catalytic activity compared to the V-based analogous catalyst and Ce^{3+} remained the dominating surface species indicating its crucial role in the reaction.[34] This is a unique characteristic of flame aerosol technology facilitating the single step production of complex multicomponent catalyst materials with desired properties such as high oxygen carrying capacity and thermal stability.

3.3 Specific surface area

Many catalytic reactions are influenced by SSA. Active metals in their bulk form possess fairly low surface areas and thus relatively little active sites per unit mass. Furthermore, catalytic active metals are prone to sintering at temperatures higher than their specific Tamman temperature. Active sites must be accessible by the reactants and therefore those located at the surface are most important because transfer to them is not limited by intraparticle diffusion. Therefore, the active components are supported on thermally stable materials such as refractory oxides (e.g. SiO$_2$, CeO$_2$, Al$_2$O$_3$, ZrO$_2$, TiO$_2$) with high SSA, resulting in high surface to volume ratio of the active component (high dispersion e.g. Pd/SiO$_2$ Fig. 5c). Flame aerosol synthesis can be considered ideal for the synthesis of high SSA materials due to fast quenching of the product, which suppresses particle growth. Flame-made V$_2$O$_5$/TiO$_2$, a widely investigated catalyst for the selective catalytic reduction of NO by NH$_3$, exhibits high NO conversion (>99%) at significantly lower temperature (200 °C). Applying VAFS, the SSA of V$_2$O$_5$/TiO$_2$ could be increased from 23 to 120 m^2 g^{-1} by increasing the oxidant flow rate (Fig. 8a),[10] as described in Section 2.3. The NO conversion over the high surface area catalysts was more than 95%, already at a low reaction temperature of about 200 °C, highlighting the importance of the catalysts' SSA. Furthermore, the increase in SSA reduced drastically the selectivity to undesired N$_2$O, an effective greenhouse gas, in the whole temperature range, as illustrated in Fig. 8a. It should be noted that such performance was achieved by scaling up the VAFS of V$_2$O$_5$/TiO$_2$ from 4 to 200 g h^{-1} as will be discussed in Section 3.8.

Maintaining constant high catalytic activity is sometimes difficult as the catalysts tend to deactivate with reaction time.
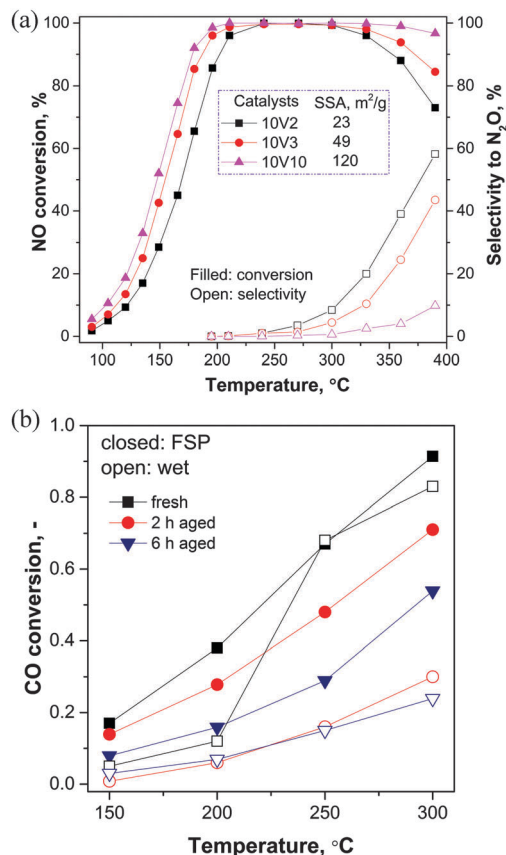

Fig. 8 (a) Effect of SSA of V$_2$O$_5$/TiO$_2$ on NO conversion (closed symbols) and N$_2$O selectivity (open symbols) in selective reduction of NO with NH$_3$. Slight improvement on NO conversion was obtained at lower reaction temperatures (<200 °C). Major influence of SSA was observed for N$_2$O selectivity, the higher SSA the lower was the selectivity (figure inset: xVy, where x: vanadia content and y: O$_2$ flow rate).[10] (b) Comparison of CO conversion over fresh (square) and hydrothermally aged (circle and down triangle) FSP (closed) and incipient wetness impregnation (IWI) (open) Mn/Al$_2$O$_3$ catalysts.[37] Adapted from ref. 10 and 37 with permission from Elsevier.

Sintering, coking and poisoning are some of the causes for catalyst deactivation.[35] Especially, with supported metal catalysts, sintering of the active component at high reaction temperatures has a major influence on catalyst activity due to increase of the crystallite size and thus lowering of the number of accessible active sites on the surface. However, in some cases sintering of a catalyst component does not necessarily lead to decreased performance. For example, Mn–Na$_2$WO$_4$/SiO$_2$ catalysts showed significant structural change, i.e. formation and growth of the cristobalite SiO$_2$ phase during the oxidative coupling of methane, but this had virtually no effect on the catalytic performance[36] indicating that the reaction is insensitive to this structural change.[35]

For reactions, however, that are sensitive to structural changes, it is important to maintain the optimal particle size and crystallite structure, by making the catalyst thermally stable. Recent work by Tepluchin et al.[37] shows that even after hydrothermal aging at 700 °C for 12 h, only a minimal decrease in SSA of FSP-made catalysts (20% Mn or 20% Fe/Al$_2$O$_3$) occurred (161 to 141 and

150 to 110 m^2 g^{-1}, respectively) compared to that of a corresponding catalysts produced by impregnation (139 to 95 and 136 to 72 m^2 g^{-1}, respectively). Manganese proved to be better than Fe for CO conversion when loaded on Al_2O_3 produced by both flame and impregnation methods. However, CO conversion over FSP-made Mn/Al_2O_3 was superior to wet-made (Fig. 8b). Though catalytic activity decreased on both catalysts after hydrothermal aging, the flame-made one still showed better performance, owing to its thermal stability. Additionally, the activity of the flame-made Mn/Al_2O_3 catalysts could be partially regenerated after SO_2 poisoning unlike the wet-made ones. This behavior was attributed to the resistance of the flame-made catalyst against sintering and poisoning, and to the homogeneous distribution of Mn species achieved.

3.4 Particle size

The influence of particle size and shape on catalyst performance is a well investigated topic. Decrease in particle size can increase the number of active sites improving the catalytic performance. Furthermore in the particle size range up to about 10 nm the statistics of atoms with a particular coordination changes significantly, which can lead to a drastic change in the catalysts' performance if the target reaction is structure-sensitive. However, controlling the size and homogenous distribution of supported nanoparticles is often difficult since the particles tend to grow by sintering, especially during prolonged high temperature calcination as used in classical wet preparation methods. Noble metals are widely used in catalysis due to their excellent catalytic properties for many reactions. However, the resources of these metals are limited as they are expensive. A viable solution towards reducing their usage would be to develop non-noble metal containing catalysts, a big challenge, or minimizing their loading while maintaining catalytic activity. Flame aerosol synthesis, where exceptional control over particle size can be achieved, is a valuable tool for targeting these challenges, as explained in Sections 2.3.

High catalytic activity can often be realized by decreasing the particle size of the active component, enhancing the interfacial contact between active (metal) particles and support. These interactions can induce electronic and geometric effects in the active particles, which are favorable for the reaction. Fig. 9 shows the influence of Pt particle size on sucrose mineralization where ∼1.6 nm sized Pt showed optimal performance regardless of reaction conditions.[38] This improved activity was attributed to the creation of additional electronic surface states and more reactive sites. Interestingly, the electronic effect induced in Pt/TiO_2 containing the smallest Pt particles (∼1.4 nm) was not favorable, since the high photocurrent density of the Pt deposits increased the electron–hole recombination. Furthermore, the deposit size was too small to establish sufficient electrical contact for efficient interfacial charge transfer between the photocatalyst and sucrose, and thus this catalyst showed relatively low activity. With increasing Pt particle size (>1.6 nm), the photocurrent started to accumulate, making formation of organic–metal deposit bonds difficult, which also resulted in low activity. In some cases, slightly larger but well-dispersed, active materials are necessary to
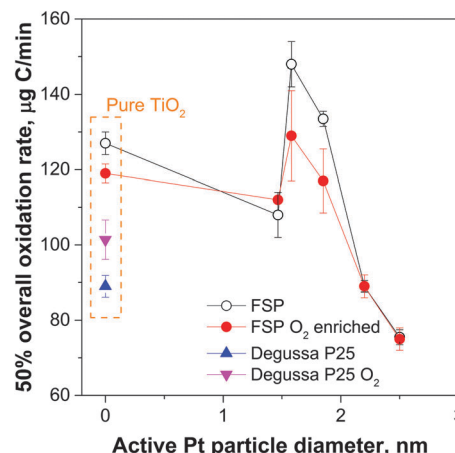

Fig. 9 Effect of active Pt particle diameter in flame-made Pt/TiO_2 on the half-life rates of 2000 μg of carbon (as sucrose) and their comparison with pure $FSP-TiO_2$ and Degussa P25. Pt particles of size ∼1.6 nm showed optimal performance.[38] Adapted from ref. 38 with permission from Elsevier.
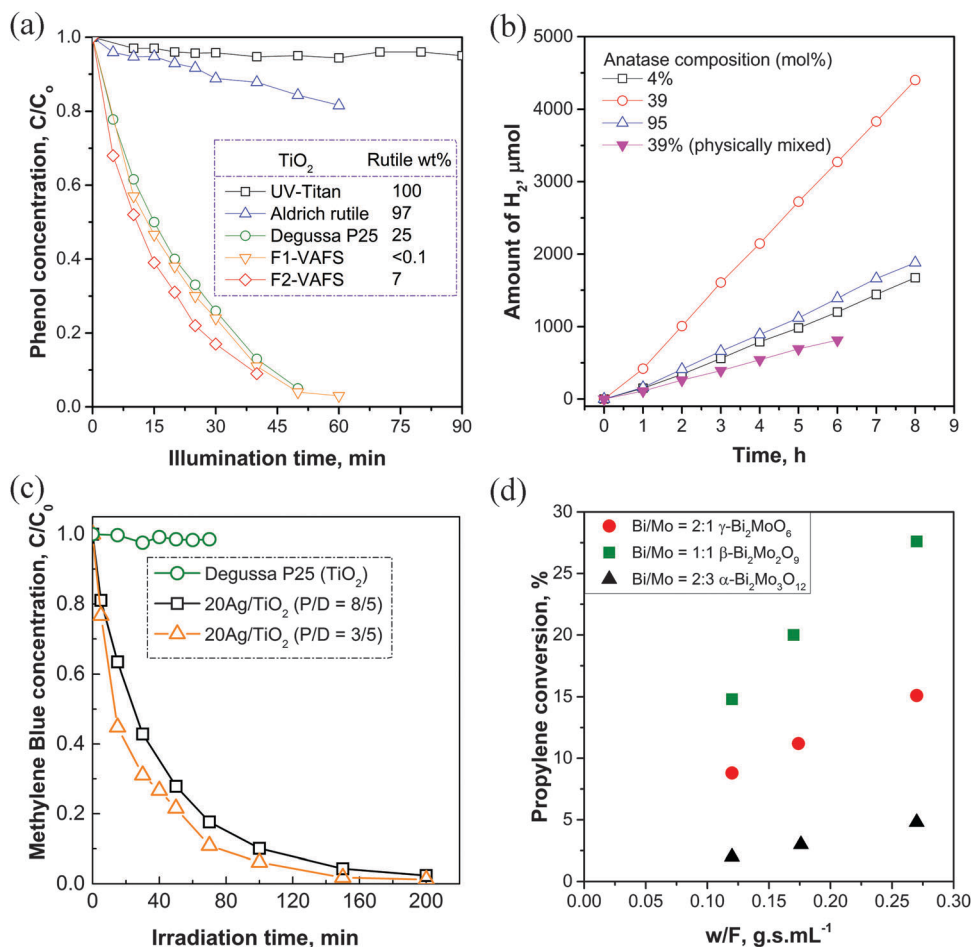
achieve high catalytic activity, as e.g. for the enantioselective hydrogenation of α-ketoesters over Rh-loaded Al_2O_3.[39]

3.5 Crystal structure and morphology

Correlating catalytic activity with crystal structure and morphology of technical catalysts is often challenging due to the difficulty in establishing a conclusive relationship. Existing differences in the physicochemical properties such as crystal composition, surface area and particle size of the analyzed materials render a proper comparison difficult. This problem can be minimized by preparing materials where all properties except the selected target property are similar. An example towards this goal is the preparation of TiO_2 with similar surface areas but different phase composition (amount of rutile) for the photocatalytic decomposition of phenol and salicylic acid[40] and the production of H_2 from methanol.[41] The comparison of the catalytic performance of flame-made TiO_2 (F1-VAFS), commercial Degussa P25 and UV-Titan, which all had similar surface areas (70–78 m^2 g^{-1}), showed that the presence of both anatase and rutile is necessary to achieve high activity (Fig. 10a).[40] The photocatalytic activity of Aldrich rutile was better than that of UV-Titan though their SSAs were vastly different (2 vs. 70 m^2 g^{-1}). This can be traced back to the presence of a small amount of anatase (3%) in the Aldrich rutile. TiO_2 particles of 20–40 nm size, which contained <10 wt% rutile, were the most photoactive in destroying phenol. Moreover, it was inferred that both anatase and rutile are necessary to achieve some activity, and a synergistic effect between them results in an optimal performing photocatalyst. Similar correlations were also observed in the photocatalytic decomposition of salicylic acid.

For the photocatalytic H_2-production from methanol also a synergistic effect between anatase and rutile was observed (Fig. 10b).[41] The optimal anatase content was 39 mol% affording a production of about 4500 μmol of H_2 in 8 h. Lower activity of the catalysts containing both higher (95 mol%) and lower (4 mol%)

3062 | Chem. Soc. Rev., 2016, 45, 3053–3068

This journal is © The Royal Society of Chemistry 2016

Fig. 10 (a) Photocatalytic decomposition of phenol with flame synthesized (F1 and F2-VAFS refers to TiO$_2$ from two different flame synthesis conditions) and commercial TiO$_2$. Initial phenol concentration: 1 mM, catalyst concentration: 0.5 g L^{-1}, pH: 3.5, O$_2$ flow rate: 1 L min^{-1}, 450 W UV-lamp.[40] (b) Photocatalytic H$_2$ evolution over flame-made TiO$_2$ nanoparticles containing different amount of anatase (4, 39, and 95 mol%) and over TiO$_2$ nanoparticles prepared by physical mixing method resulting in 39% anatase.[41] (c) Photocatalytic reduction of methylene blue by Degussa P25 and Ag/TiO$_2$ prepared by FSP at P/D = 8/5 and 3/5 under visible-light irradiation (λ > 400 nm).[42] (d) Propylene conversion as a function of contact time (w/F) over flame-made Bi/Mo catalysts.[45] Adapted from ref. 40, 41, 42 and 45 with permission from Taylor & Francis, American Chemical Society, Elsevier and Royal Society of Chemistry.

anatase content further substantiated the necessity of optimal composition. Interestingly, mechanical mixing of TiO$_2$, mimicking optimal anatase content (39 mol%), afforded the lowest activity, which can be attributed to the absence of a beneficial synergistic effect, as it was observed with the flame-made catalysts. In addition to the control over the content of these conventional TiO$_2$ phases, metastable phases such as crystalline Ti$_3$O$_5$ and Ti$_4$O$_7$ can also be produced by FSP.[42] These titanium suboxides were discovered in flame-made Ag/TiO$_2$ that showed very high visible-light activity for the photodegradation of Cr^{6+} and methylene blue (down to 15 min half-life) compared to that of conventional P25 (Fig. 10c).

The possibility of the formation of these types of metastable phases and crystal structures by flame aerosol synthesis provides an interesting tool for tailoring materials suitable for catalytic application. Another example is the preparation of low temperature BaCO$_3$ that was produced by applying two-nozzle synthesis. This material exhibits high NO$_x$ storage capacity.[6]

Moreover, successful production of Pt–Ba/Al$_2$O$_3$ catalysts virtually free of the high temperature BaCO$_3$, in a wide range of Ba loadings (4.5–33 wt%), led to improved NO$_x$ storage capacity of these catalysts. In contrast, wet-made catalyst of similar composition contained high temperature BaCO$_3$ that led to lower NO$_x$ storage capacity compared to flame-made ones.[43] Other studies indicate that higher dispersion of active species can be achieved by flame aerosol synthesis compared to classical wet-chemistry methods, resulting in higher catalytic activity, e.g. V$_2$O$_5$/TiO$_2$ for methanol oxidation.[44]

Metastable phases such as β-Bi$_2$Mo$_2$O$_9$ with high SSA (19 m^2 g^{-1}) can also be synthesized in a single step using FSP.[45] Generally, this phase is obtained by a high temperature (> 560 °C) calcination process that results in low SSA. Propylene conversion over this metastable phase was higher than that of other phases (α-Bi$_2$Mo$_3$O$_{12}$ and γ-Bi$_2$MoO$_6$) and increased with increasing contact time (Fig. 10d). Acrolein selectivity of all these catalysts was comparable (all around 70%) at their

This journal is © The Royal Society of Chemistry 2016

Chem. Soc. Rev., 2016, 45, 3053–3068 | 3063

highest conversion proving the superior catalytic performance of β-Bi$_2$Mo$_2$O$_9$. The catalytic activity of both α- and γ-phases was lower than that of the β-phase though their SSAs were similar (α-phase, 18 m^2 g^{-1}) or even higher (γ-phase, 45 m^2 g^{-1}) than that of the β-phase (19 m^2 g^{-1}), illustrating the role of crystal structure in the reaction. These metastable or mixed-oxide phases are formed in flame aerosol synthesis due to rapid quenching of the particles that immediately leads to freezing of the structure.

3.6 Spatial distribution of components

The nature and location of active catalyst components either on the surface or in the subsurface of the support can greatly influence the catalytic activity. In flame synthesis of Pt–Pd/Al$_2$O$_3$ catalysts, an alloy of Pt–Pd was formed, confirmed by EDXS (Fig. 5d) and EXAFS analyses.[46] Catalytic activity of the combustion of CH$_4$ was high over the catalysts containing Pt–Pd alloy as Pt influenced the redox property of Pd favoring its presence in reduced form. The H$_2$-TPR results showed that Pt addition broadens the Pd reduction signal and shifts it towards lower temperatures, indicating easier reduction. A small increase of the Pt content of the catalyst improved its resistance towards sintering thus enhancing the CH$_4$ combustion activity.

In flame-made Co/ZrO$_2$, Co was internally distributed and stabilized within the ZrO$_2$ matrix, unlike in conventionally prepared catalysts.[47] This facilitated formation of very fine Co^0 clusters after the reduction and their amount was doubled after addition of a small quantity (0.4 wt%) of noble metal (Ag, Ru, Pt, Rh, Pd) as promoter, enhancing the reducibility of the Co-species. The high temperature CoO$_x$ reduction peak shifted from about 550 °C to around 320 °C except in the case of Ag promotion. Rh addition to Co/ZrO$_2$ ameliorated the hydrogenation of CO and resulted in higher methane selectivity with increasing hydrogen partial pressure compared to the unpromoted catalyst.

As the number of components in the catalyst increases, the complexity in understanding the underlying reasons for the catalyst activity also increases due to their interdependent interactions. Therefore, control over the location/interaction of these components can provide a better understanding of the function of catalysts and eventually aid in the design of optimal performing catalysts. In this case, two-nozzle synthesis can be applied for developing sophisticated materials where the intermixing and interaction of the different components in the flame can be better controlled.[6]

Formation of mixed oxides is favored in single nozzle systems due to the homogeneous distribution of the precursor components in the feed, which results in intimate mixing in the flame, while this intermixing can be minimized with two nozzles systems.[6] Spraying Pt/Ba and Al$_2$O$_3$ precursor separately utilizing two nozzles, crystalline BaCO$_3$ was obtained, whereas it was amorphous in powders prepared by single-nozzle synthesis. Moreover, BaCO$_3$ crystallinity could be improved by increasing the inter-nozzle distance, which delays the intermixing of Ba and Al, and consequently the interaction occurs at lower temperature. Higher NO$_x$ uptake by Pt/Ba/Al$_2$O$_3$ catalyst prepared by two nozzles

(3.6% vs. 0.9 wt%) demonstrated the beneficial use of two-nozzle synthesis in this case.

Fig. 11a shows schematically the two-nozzle set-up as it was used for the spatial control of the different components of potassium promoted Pt/Al$_2$O$_3$ and Pd/Al$_2$O$_3$ NO$_x$ storage–catalysts. The precursor solution of the desired components could be sprayed separately, e.g. by spraying solution mixture containing precursors of potassium (K) and Pt or Pd with one nozzle and precursor solution containing only Al with the other.[48] As a result, catalysts with spatially controlled deposition were obtained where Pt or Pd are interacting preferentially with K$_2$CO$_3$, or catalysts where the noble metals were deposited on Al$_2$O$_3$ instead on K$_2$CO$_3$.

Using this set-up, during synthesis, particle size, composition and location of the individual components can be controlled to some extent. The particles produced from each nozzle condense first before mixing to the final product, promoting mixing at the nanoscale rather than on atomic scale[6] ensuring their predetermined interactions and location. By variation of the intersection distance between the two nozzles, catalyst can be optimized based on the feedback of performance tests. Utilizing this technique, it was shown that Pd deposition on Al$_2$O$_3$ and Pt on
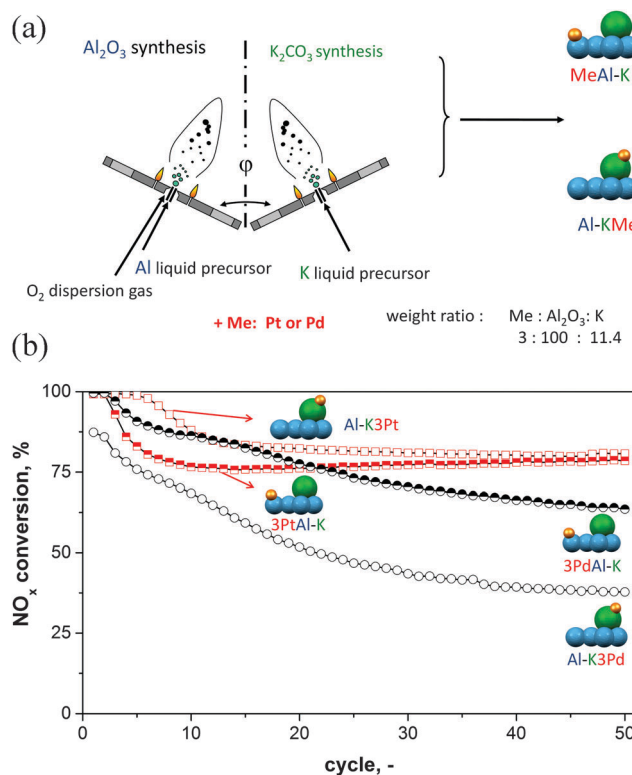
Fig. 11 (a) Schematic of two-nozzle flame synthesis configurations leading to preferential deposition of Pt/Pd on K$_2$CO$_3$ or Al$_2$O$_3$. (b) Performance of catalysts prepared by preferential deposition in NO storage–reduction at 250 °C. NO$_x$ conversion as a function of lean-rich cycling of catalysts. Each cycle consisted of a lean (oxidizing) period (3 min in 667 ppm NO and 3.3% O$_2$ in He) and a rich (reducing) period (1 min in 667 ppm NO and 1333 ppm C$_3$H$_6$ in He). The highest NO$_x$ conversion was observed for catalyst with Pt on K$_2$CO$_3$ and Pd deposited on Al$_2$O$_3$.[48] Adapted from ref. 48 with permission from Elsevier.

K_2CO_3 exhibits best performance for NO_x storage–reduction, especially at the beginning of the cycling between fuel-lean and fuel-rich periods (Fig. 11b).[48]

Novel highly active Pt/FeO_x–CeO_2 catalysts for the preferential oxidation of carbon monoxide (PROX) were developed by adjusting the intersection distance between the two nozzles that controlled the interactions between Pt/FeO_x and CeO_2.[49] Strong inter-action between Pt and FeO_x was evident by electron microscopy (Pt residing in FeO_x crystals Fig. 5e). By adjusting the intersection distance, it was possible to tune the morphology and the redu-cibility of the catalysts. Intimate interactions between Pt/FeO_x and CeO_2 achieved at the greatest flame distance led to reduci-bility of the material at the lowest temperature (-6 °C). This tailor-made catalyst showed CO conversion $>99.5\%$ below 90 °C, which is 30 °C lower than that of mechanically mixed catalyst of same composition.

Co–Mo/Al_2O_3 catalysts for hydrodesulfurization (HDS) were prepared employing single-nozzle and two-nozzle FSP.[50] The best performing catalysts were those prepared with the two-nozzle FSP, which showed an improve of the relative activity, compared to a commercial reference catalyst, of 91% while the corresponding single-nozzle made catalyst showed a relative activity of 75%. The better performance of the catalyst prepared by two-nozzle FSP was attributed to better promotion of the active molybdenum sulfide phase, due to suppression of the formation of the undesired phase $CoAl_2O_4$, which makes Co unavailable for promotion.

The above examples illustrate that prior knowledge of the required physical and chemical properties of the catalyst is essential in choosing the right synthesis method.

Another important advantage of the two-nozzle synthesis is that it overcomes the problem of precursor immiscibility, because the solvent can be adopted to the solubility of the precursor. The extension of the two-nozzle system to systems containing further nozzles is feasible. However, to benefit from such an extension, a better understanding of the particle formation mechanism in multicomponent system is crucial.

3.7 Coating of ceramic supports

Structured ceramic supports have found wide application, particularly in environmental catalysis. Generally, the catalytic powders are wash-coated on cordierite honeycomb and thermally treated at high temperatures before using them in a catalytic process, e.g. in exhaust gas treatments. This requires various steps, and a lengthy process, which leads to significant fabri-cation costs. Therefore, development of a technique that can directly coat the catalytic materials onto the ceramic support, which also avoids post-thermal treatment, will be beneficial for many catalyst industries. The flame aerosol technique can be utilized for developing such catalyst-coated ceramic supports, as has been demonstrated by Schimmoeller et al.[51] The ceramic foam was mounted into a double-walled water cooled tube and positioned right above the flame producing V_2O_5/TiO_2 (Fig. 12a),
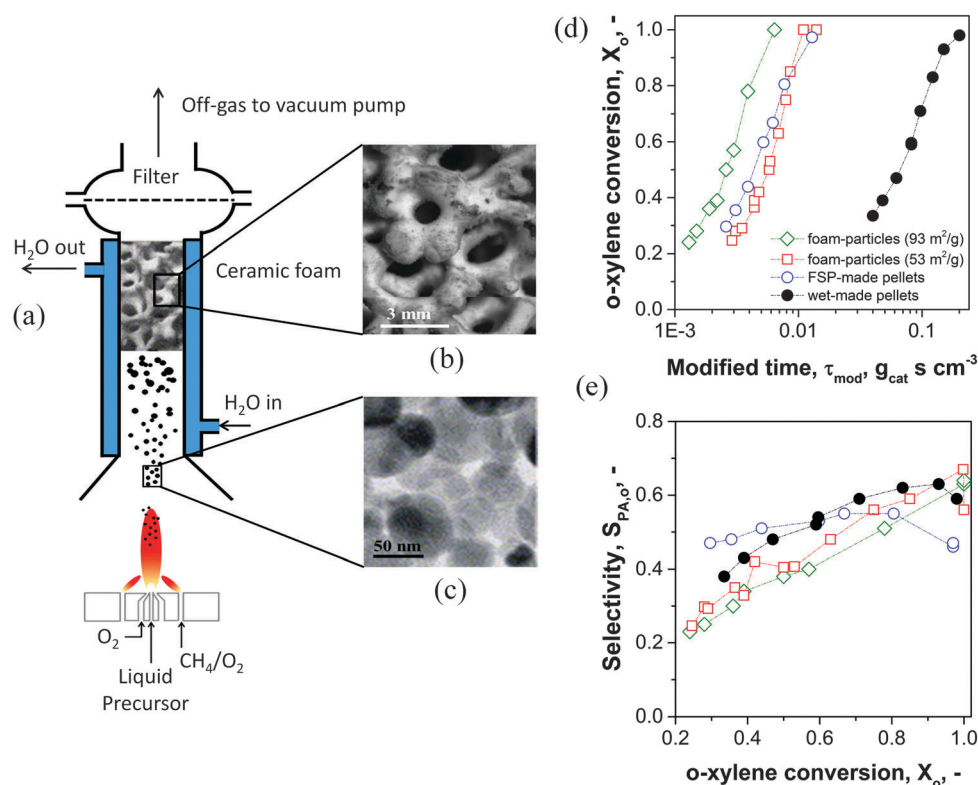
Fig. 12 (a) Schematic of the FSP coating of V_2O_5/TiO_2 catalyst onto ceramic foam, (b) SEM image of catalyst coated ceramic foam and (c) TEM image of V_2O_5/TiO_2 nanoparticles. (d and e) Catalytic performance of various coated ceramic foams and pellets in o-xylene oxidation to phthalic anhydride. (d) o-xylene conversion with modified time and (e) o-xylene conversion versus phthalic anhydride selectivity.[51] Adapted from ref. 51 with permission from Elsevier.

This journal is © The Royal Society of Chemistry 2016

Chem. Soc. Rev., 2016, 45, 3053–3068 | 3065

which was tested in the partial oxidation of *o*-xylene to phthalic anhydride. The coating amount was easily controlled by varying the pressure drop and deposition time. Homogeneous coating was achieved (Fig. 12b) and the catalyst powder coating showed a homogeneous particle size distribution (Fig. 12c). The coated foam with high SSA (93 m^2 g^{-1}) exhibited significantly higher activity compared to that of the coated foam with low SSA (53 m^2 g^{-1}) and pelletized (both FSP- and wet-made) catalysts (Fig. 12d). Moreover, coated forms showed higher phthalic anhydride selectivity than that of others at 100% *o*-xylene conversion (Fig. 12e). The high catalytic activity of the coated ceramics was attributed to the high SSA and porosity (∼98%) that enhanced the intraparticle mass transfer, which was suppressed in pelletized catalysts of similar composition due to their longer diffusion path and smaller pore sizes.

Direct deposition of Mn$_3$O$_4$ onto catalytic laboratory-scaled cordierite diesel particulate filter was tested for soot oxidation using FSP.[52] The oxidation of tight contact soot occurred in the temperature range of 180–350 °C, which indicates its potential for instantaneous removal of soot under these conditions. As a result, particulate filter could be continuously regenerated under realistic diesel exhaust conditions. The investigations discussed above are promising and this novel direct catalyst coating technology using flame methods is likely to be attractive for catalyst industries.

3.8 Scale-up

An important feature of any synthesis process is its scalability while maintaining the physicochemical properties of the best catalyst emerging from laboratory tests. While many synthesis methods show significant hurdles for scale-up, flame aerosol synthesis is already a proven scale-up technology, as *e.g.* demonstrated by the industrial scale production of photo-catalytic TiO$_2$.[1] Physicochemical properties of the material are strongly influenced by process parameters as described in Section 2.3. Therefore, it requires a proper understanding of the process from both experimental observations and theoretical simulations. Understanding of the whole synthesis process is a prerequisite for successful scale-up. Recently, Gröhn *et al.*[20] demonstrated that ZrO$_2$ nanoparticles production can be scaled-up from ∼100 to 500 g h^{-1} by maintaining important product properties such as crystal size and type. This was achieved by keeping the high temperature residence time constant during the synthesis *i.e.* maintaining the FSP *P/D* ratio constant (Fig. 13a). Variation of the *P/D* ratio had virtually no effect on the mass fraction of tetragonal ZrO$_2$ (92–96 wt%) except that the crystal size increased from about 10 to 22 nm.

The possibility of large scale production of materials such as SiO$_2$ (>1000 g h^{-1}), ZrO$_2$ (up to 600 g h^{-1}) and Y$_2$O$_3$/ZrO$_2$ (>300 g h^{-1}) utilizing FSP has already been demonstrated by various authors as has been summarized in a recent study.[20] In addition, ZnO nanorods can also be produced using FSP in high production rates (>3 kg h^{-1}, Fig. 5f).[53] It seems justified to state that multicomponent catalysts production can also be scaled-up maintaining the physicochemical properties and thus in several cases the flame aerosol technique can potentially
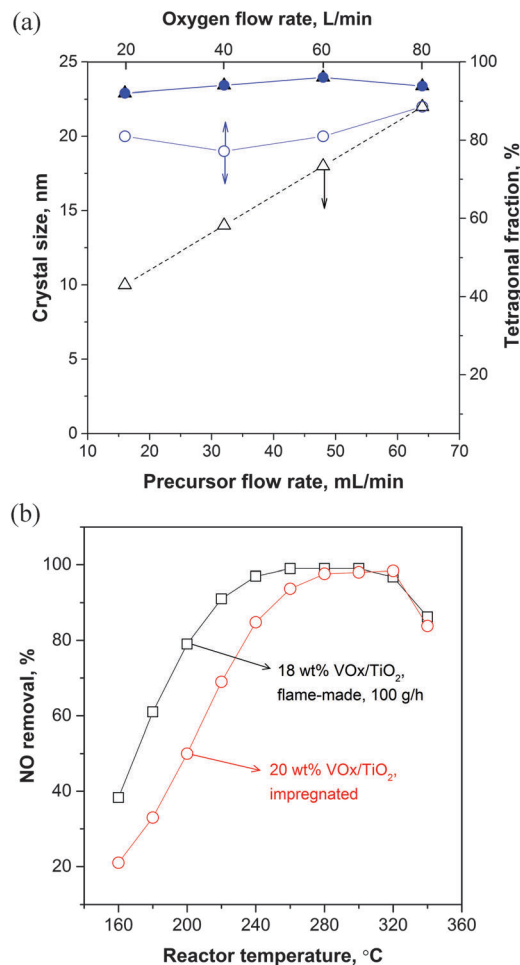
Fig. 13 (a) Product ZrO$_2$ tetragonal phase fraction (right axis, solid symbols) and crystal size (left axis, open symbols) as a function of precursor flow at constant 80 L min^{-1} of O$_2$ (triangles) and constant precursor to dispersion O$_2$ (*P/D*) flow ratio (circles). Product crystallinity is maintained during constant *P/D* ratio scaling.[20] (b) Catalytic activity comparison of flame- and wet-made V$_2$O$_5$/TiO$_2$ catalysts for the NO removal by selective catalytic reduction. Flame-made catalyst production was scaled up to 100 g h^{-1} and its catalytic performance was superior to that of the catalyst prepared using wet-impregnation method.[54] Adapted from ref. 20 and 54 with permission from American Chemical Society and John Wiley & Sons.

replace the time consuming wet-synthesis methods. Successful pilot scale production of binary catalyst (V$_2$O$_5$/TiO$_2$) has already been demonstrated using a diffusion flame reactor (VAFS) with a high production rate of 200 g h^{-1}.[54] The catalyst showed better NO removal activity (160–280 °C) compared to a corresponding one with similar composition and SSA produced by classical wet-chemistry method (Fig. 13b).

4. Concluding remarks

The flame aerosol technique is an attractive route for nano-particle synthesis, which already is employed in many powder synthesis industries and is currently being explored by many academic and industrial laboratories for catalysis. However, there are still challenges in this technique, one of them being

3066 | *Chem. Soc. Rev.*, 2016, **45**, 3053–3068

This journal is © The Royal Society of Chemistry 2016

precursor costs. Ideal precursors (*e.g.* alkoxides, organometallic compounds) are relatively expensive, while cheaper and therefore preferred nitrate precursors usually give inhomogeneous particles that are not desirable. However, utilizing proper chemistry, homogeneous catalytic particles could be produced[55] from these cheap precursors opening up new avenues for utilizing a wide range of inexpensive precursors for catalyst production.

Standard methodology for the inflight characterization of the aggregates and agglomerates is necessary as it affects the assessment of the particle growth processes, which in-turn affects their performance. Modification of nanoparticle surface with functional materials (organic groups) during their production is another aspect that can be explored. Development and successful implementation of such process can cut the cost of post functionalization. Scale-up of material production is a challenge for many synthesis techniques due to limited understanding of the dynamics involved in the production of homogeneous multicomponent materials. In contrast, scalability of flame technology is already proven in the production of nanomaterials.[2,20] Forced nozzle quenching can be utilized to reduce the particle size (*e.g.* TiO_2).[16] This possibility could be further explored in the synthesis of catalysts. Utilizing the flame aerosol technique, synthesis of non-oxygen containing metal fluorides, sulfides, nitrides, carbides and phosphides could be feasible provided that O_2 is controlled in the synthesis environment.

Flame aerosol synthesis produces non-porous nanoparticles and also less crystalline products, due to low particle residence time in the high temperature zone of the flame. Therefore, this technique may not be suitable for catalytic reactions where these properties of the nanoparticles are crucial. However, by controlling the air entrainment and the length of the tube enclosing the flame,[18] crystallinity of the particles can be improved by manipulating their residence time at high temperatures.[5] Today, only a few investigations[51,52] show the possibility of developing direct catalyst coating technique utilizing FSP. However, these examples show the feasibility and potential of this technique.

The future of this synthesis technique for the production of various sophisticated materials with application not only in catalysis seems promising. This is also reflected by a significant increase of the research activity in this field witnessed in the past few years. However, more work will be required to fully understand the chemical and physical processes occurring in the flame and to fully exploit the potential of this technique for material synthesis. Research towards this aim will need a concerted effort of material scientists, chemists, physicists and engineers.

Acknowledgements

References

1 G. D. Ulrich, *Chem. Eng. News*, 1984, **62**, 22–29.
2 S. E. Pratsinis, *Prog. Energy Combust. Sci.*, 1998, **24**, 197–219.
3 R. Strobel, A. Baiker and S. Pratsinis, *Adv. Powder Technol.*, 2006, **17**, 457–480.
4 J. A. Schwarz, C. Contescu and A. Contescu, *Chem. Rev.*, 1995, **95**, 477–510.
5 S. E. Pratsinis, W. Zhu and S. Vemury, *Powder Technol.*, 1996, **86**, 87–93.
6 R. Strobel, L. Mädler, M. Piacentini, M. Maciejewski, A. Baiker and S. E. Pratsinis, *Chem. Mater.*, 2006, **18**, 2532–2537.
7 R. Strobel and S. E. Pratsinis, *J. Mater. Chem.*, 2007, **17**, 4743–4756.
8 B. Schimmoeller, S. E. Pratsinis and A. Baiker, *ChemCatChem*, 2011, **3**, 1234–1256.
9 S. Tsantilis and S. E. Pratsinis, *Langmuir*, 2004, **20**, 5933–5939.
10 W. J. Stark, K. Wegner, S. E. Pratsinis and A. Baiker, *J. Catal.*, 2001, **197**, 182–191.
11 M. Sokolowski, A. Sokolowska, A. Michalski and B. Gokieli, *J. Aerosol Sci.*, 1977, **8**, 219–230.
12 B. S. Marshall, I. Telford and R. Wood, *Analyst*, 1971, **96**, 569–578.
13 L. Mädler, H. K. Kammler, R. Mueller and S. E. Pratsinis, *J. Aerosol Sci.*, 2002, **33**, 369–389.
14 R. Strobel, W. J. Stark, L. Mädler, S. E. Pratsinis and A. Baiker, *J. Catal.*, 2003, **213**, 296–304.
15 B. Thiébaut, *Platinum Met. Rev.*, 2011, **55**, 149–151.
16 K. Wegner and S. E. Pratsinis, *AIChE J.*, 2003, **49**, 1667–1675.
17 P. Demokritou, R. Büchel, R. M. Molina, G. M. Deloid, J. D. Brain and S. E. Pratsinis, *Inhalation Toxicol.*, 2010, **22**, 107–116.
18 O. Waser, A. J. Groehn, M. L. Eggersdorfer and S. E. Pratsinis, *Aerosol Sci. Technol.*, 2014, **48**, 1195–1206.
19 W. J. Stark, L. Madler, M. Maciejewski, S. E. Pratsinis and A. Baiker, *Chem. Commun.*, 2003, 588–589.
20 A. J. Gröhn, S. E. Pratsinis, A. Sánchez-Ferrer, R. Mezzenga and K. Wegner, *Ind. Eng. Chem. Res.*, 2014, **53**, 10734–10742.
21 E. K. Athanassiou, F. Krumeich, R. N. Grass and W. J. Stark, *Phys. Rev. Lett.*, 2008, **101**, 166804.
22 W. J. Stark, R. Strobel, D. Gunther, S. E. Pratsinis and A. Baiker, *J. Mater. Chem.*, 2002, **12**, 3620–3625.
23 F. Hoxha, B. Schimmoeller, Z. Cakl, A. Urakawa, T. Mallat, S. E. Pratsinis and A. Baiker, *J. Catal.*, 2010, **271**, 115–124.
24 J. Huang, Y. Jiang, N. van Vegten, M. Hunger and A. Baiker, *J. Catal.*, 2011, **281**, 352–360.
25 Z. Wang, Y. Jiang, M. Hunger, A. Baiker and J. Huang, *ChemCatChem*, 2014, **6**, 2970–2975.
26 Y. Jiang, J. Scott and R. Amal, *Appl. Catal., B*, 2012, **126**, 290–297.
27 G. L. Chiarello, M. V. Dozzi, M. Scavini, J.-D. Grunwaldt and E. Selli, *Appl. Catal., B*, 2014, **160–161**, 144–151.
28 B. Weidenhof, M. Reiser, K. Stöwe, W. F. Maier, M. Kim, J. Azurdia, E. Gulari, E. Seker, A. Barks and R. M. Laine, *J. Am. Chem. Soc.*, 2009, **131**, 9207–9219.
29 M. Kim and R. M. Laine, *J. Am. Chem. Soc.*, 2009, **131**, 9220–9229.

This journal is © The Royal Society of Chemistry 2016

Chem. Soc. Rev., 2016, **45**, 3053–3068 | 3067

30 G. L. Chiarello, I. Rossetti and L. Forni, *J. Catal.*, 2005, **236**, 251–261.

31 O. Buchneva, I. Rossetti, C. Oliva, M. Scavini, S. Cappelli, B. Sironi, M. Allieta, A. Kryukov and L. Forni, *J. Mater. Chem.*, 2010, **20**, 10021–10031.

32 S. Roy, N. van Vegten, N. Maeda and A. Baiker, *Appl. Catal., B*, 2012, **119–120**, 279–286.

33 N. van Vegten, T. Baidya, F. Krumeich, W. Kleist and A. Baiker, *Appl. Catal., B*, 2010, **97**, 398–406.

34 K. A. Michalow-Mauke, Y. Lu, K. Kowalski, T. Graule, M. Nachtegaal, O. Kröcher and D. Ferri, *ACS Catal.*, 2015, **5**, 5657–5672.

35 C. H. Bartholomew, *Appl. Catal., A*, 2001, **212**, 17–60.

36 R. Koirala, R. Büchel, S. E. Pratsinis and A. Baiker, *Appl. Catal., A*, 2014, **484**, 97–107.

37 M. Tepluchin, S. Kureti, M. Casapu, E. Ogel, S. Mangold and J. D. Grunwaldt, *Catal. Today*, 2015, **258**, 498–506.

38 W. Y. Teoh, L. Mädler, D. Beydoun, S. E. Pratsinis and R. Amal, *Chem. Eng. Sci.*, 2005, **60**, 5852–5861.

39 F. Hoxha, N. van Vegten, A. Urakawa, F. Krumeich, T. Mallat and A. Baiker, *J. Catal.*, 2009, **261**, 224–231.

40 G. P. Fotou and S. E. Pratsinis, *Chem. Eng. Commun.*, 1996, **151**, 251–269.

41 Y. K. Kho, A. Iwase, W. Y. Teoh, L. Mädler, A. Kudo and R. Amal, *J. Phys. Chem. C*, 2010, **114**, 2821–2829.

42 K. Fujiwara, Y. Deligiannakis, C. G. Skoutelis and S. E. Pratsinis, *Appl. Catal., B*, 2014, **154–155**, 9–15.

43 M. Piacentini, R. Strobel, M. Maciejewski, S. E. Pratsinis and A. Baiker, *J. Catal.*, 2006, **243**, 43–56.

44 V. Kumar, N. Lee and C. B. Almquist, *Appl. Catal., B*, 2006, **69**, 101–114.

45 K. Schuh, W. Kleist, M. Hoj, V. Trouillet, A. D. Jensen and J. D. Grunwaldt, *Chem. Commun.*, 2014, **50**, 15404–15406.

46 R. Strobel, J.-D. Grunwaldt, A. Camenzind, S. Pratsinis and A. Baiker, *Catal. Lett.*, 2005, **104**, 9–16.

47 W. Y. Teoh, D. E. Doronkin, G. K. Beh, J. A. H. Dreyer and J.-D. Grunwaldt, *J. Catal.*, 2015, **326**, 182–193.

48 R. Büchel, S. E. Pratsinis and A. Baiker, *Appl. Catal., B*, 2011, **101**, 682–689.

49 J. A. H. Dreyer, H. K. Grossmann, J. Chen, T. Grieb, B. B. Gong, P. H. L. Sit, L. Mädler and W. Y. Teoh, *J. Catal.*, 2015, **329**, 248–261.

50 M. Høj, D. Pham, M. Brorson, L. Mädler, A. Jensen and J.-D. Grunwaldt, *Catal. Lett.*, 2013, **143**, 386–394.

51 B. Schimmoeller, H. Schulz, S. E. Pratsinis, A. Bareiss, A. Reitzmann and B. Kraushaar-Czarnetzki, *J. Catal.*, 2006, **243**, 82–92.

52 S. Wagloehner, M. Nitzer-Noski and S. Kureti, *Chem. Eng. J.*, 2015, **259**, 492–504.

53 K. Hembram, D. Sivaprakasam, T. N. Rao and K. Wegner, *J. Nanopart. Res.*, 2013, **15**, 1–11.

54 W. J. Stark, A. Baiker and S. E. Pratsinis, *Part. Part. Syst. Charact.*, 2002, **19**, 306–311.

55 T. Biemelt, K. Wegner, J. Teichert and S. Kaskel, *Chem. Commun.*, 2015, **51**, 5872–5875.